

## FAST DIRECTIONAL CORRELATION ON THE SPHERE WITH STEERABLE FILTERS

Y. WIAUX<sup>1</sup>

Signal Processing Institute, Ecole Polytechnique Fédérale de Lausanne (EPFL), CH-1015 Lausanne, Switzerland

L. JACQUES

Institut de Physique théorique, Université catholique de Louvain (UCL), B-1348 Louvain-la-Neuve, Belgium

P. VIELVA

Instituto de Física de Cantabria (CSIC-UC), E-39005 Santander, Spain; and Astrophysics Group, Cavendish Laboratory, University of Cambridge, CB3 0HE Cambridge, United Kingdom

AND

P. VANDERGHEYNST

Signal Processing Institute, Ecole Polytechnique Fédérale de Lausanne (EPFL), CH-1015 Lausanne, Switzerland

*Draft version November 9, 2018*

### ABSTRACT

A fast algorithm is developed for the directional correlation of scalar band-limited signals and band-limited steerable filters on the sphere. The asymptotic complexity associated to it through simple quadrature is of order  $\mathcal{O}(L^5)$ , where  $2L$  stands for the square-root of the number of sampling points on the sphere, also setting a band limit  $L$  for the signals and filters considered. The filter steerability allows to compute the directional correlation uniquely in terms of direct and inverse scalar spherical harmonics transforms, which drive the overall asymptotic complexity. The separation of variables technique for the scalar spherical harmonics transform produces an  $\mathcal{O}(L^3)$  algorithm independently of the pixelization. On equi-angular pixelizations, a sampling theorem introduced by Driscoll and Healy implies the exactness of the algorithm. The equi-angular and HEALPix implementations are compared in terms of memory requirements, computation times, and numerical stability. The computation times for the scalar transform, and hence for the directional correlation, of maps of several megapixels on the sphere ( $L \simeq 10^3$ ) are reduced from years to tens of seconds in both implementations on a single standard computer. These generic results for the scale-space signal processing on the sphere are specifically developed in the perspective of the wavelet analysis of the cosmic microwave background (CMB) temperature ( $T$ ) and polarization ( $E$  and  $B$ ) maps of the WMAP and Planck experiments. As an illustration, we consider the computation of the wavelet coefficients of a simulated temperature map of several megapixels with the second Gaussian derivative wavelet.

*Subject headings:* cosmology: cosmic microwave background — methods: data analysis — methods: numerical

### 1. INTRODUCTION

The cosmic microwave background (CMB) temperature and polarization anisotropy distribution represents today an exceptional cosmological laboratory for the study of the geometrical structure, energy content, and evolution of the universe. The last fifteen years of detection and analysis, culminating with the all-sky maps of the Wilkinson Microwave Anisotropy Probe (WMAP) satellite mission, has led to a rather precise determination of the corresponding cosmological parameters, defining the concordance cosmological model (Page et al. 2003; Spergel et al. 2003; Spergel et al. 2006). The universe is assumed to be globally homogeneous and isotropic (cosmological principle) and the CMB anisotropies arise from Gaussian quantum fluctuations defined in a primordial inflationary era. From the signal processing point of view, the CMB is therefore a unique realization of a Gaussian and stationary (homogeneous and isotropic) random process on the celestial sphere and may be completely studied in terms of its temperature and polarization angular power spectra. The concordance cosmological model is defined by the values of the cosmological parameters giving the angu-

lar power spectra which best fit the experimental data. However, among other assumptions, the basic theoretical hypotheses of Gaussianity and stationarity of the signal must imperatively be thoroughly tested before the concordance model may be trusted. Many approaches have been proposed in this direction. In particular, the analysis of local features in the CMB temperature and polarization anisotropies might reveal either signatures of fundamental non-Gaussianity or statistical anisotropy, or foreground emissions. The scale-space analysis of the CMB, *i.e.* the combined analysis of scale and localization of features in the signal, is therefore of fundamental interest. In that perspective, the efficiency of the wavelet signal processing of the CMB has already been established. First results have also been obtained from the wavelet analysis of the WMAP all-sky temperature data, notably in (Vielva et al. 2004; Mukherjee & Wang 2004; McEwen et al. 2005a; Cruz et al. 2005).

A practical approach to wavelets on the sphere was recently introduced in that context of scale-space analysis of the CMB (Wiaux et al. 2005). In the proposed formalism, the analysis of a signal is performed through its wavelet coefficients, resulting from the directional correlation of the signal with a localized filter to which dilations, rotations, and translations

<sup>1</sup> yves.wiaux@epfl.ch

may be applied. Analogously to the corresponding formalism on the plane, wavelet filters on the sphere must satisfy an admissibility condition which guarantees that any signal may be explicitly reconstructed from its wavelet coefficients. A correspondence principle was also established, which states that the inverse stereographic projection of a wavelet on the plane gives a wavelet on the sphere. This correspondence principle enables to transfer properties, such as the filter directionality and steerability, from the plane onto the sphere. Any non-axisymmetric filter is said to be directional. The good directionality of a filter may be measured in terms of the peakedness of its auto-correlation function. The steerability of a filter is that property through which an arbitrary rotation of the filter around itself may be computed exactly in terms of a finite number of basis filters (Wiaux et al. 2005).

The present work develops a fast algorithm for the directional correlation of band-limited signals and band-limited steerable filters on the sphere, in particular wavelet filters. In the context of the scale-space CMB analysis, this algorithm reduces typical computation times for the directional correlation of all-sky maps of several megapixels from the ongoing WMAP or the forthcoming Planck missions from years to tens of seconds, thus rendering them easily affordable. The scale-space wavelet analysis of the CMB temperature ( $T$ ) and polarization ( $E$  and  $B$ ) anisotropies, and in particular the identification of possible local non-Gaussianity or statistical anisotropy signatures, or foreground emissions, is thereby accessible with the same high precision in both position and direction. The proposed algorithm may also be directly applied in the study of beam asymmetry effects on the CMB temperature and polarization data (Challinor et al. 2000; Wandelt & Górski 2001; Ng 2005). But the generic results exposed for the directional correlation on the sphere may actually find applications in many other fields beyond cosmology (Bülow & Daniilidis 2001; Bülow 2002).

In § 2, we define the directional correlation on the sphere as the scalar product of a signal and a directional filter at all possible positions of the filter on the sphere, and for all possible directions at each point. It is therefore a function defined on the rotation group in three dimensions  $SO(3)$ . By opposition, the standard correlation on the sphere considers a fixed direction of the filter and is associated with a function on the sphere  $S^2$ . We discuss the *a priori*  $\mathcal{O}(L^5)$  asymptotic complexity for the computation of the directional correlation through simple quadrature, where  $2L$  stands for the square-root of the number of sampling points on the sphere, also setting a band limit  $L$  for the signals and filters considered. The corresponding naive computation of the directional correlation would take several years on a single standard computer for fine samplings on the sphere of order  $L \simeq 10^3$ , and is thus inaccessible in terms of computation times. We then recall that the spherical harmonics and the Wigner  $D$ -functions form orthogonal bases in the spaces of square-integrable functions on  $S^2$  and  $SO(3)$  respectively. We also introduce a relation giving the directional correlation as the inverse Wigner  $D$ -functions transform of the pointwise product between the signal and filter scalar spherical harmonics coefficients. In § 3, we recall the notion of steerable filters on the sphere, and give the examples of the first and second Gaussian derivatives. We also show that the directional correlation of arbitrary signals with steerable filters is explicitly given in terms of the standard correlations with their basis filters. We briefly introduce spin-weighted spherical harmonics as orthonormal bases for the decompo-

sition of spin functions on the sphere and derive a natural relation giving the standard correlation as a sum of inverse spin-weighted spherical harmonics transforms. In § 4, we explicitly define our algorithm. We first discuss the global algorithmic structure, as well as pixelization choices. We then establish a recurrence relation which expresses spin-weighted spherical harmonics as linear combinations of scalar spherical harmonics. Consequently, the directional correlation of a scalar function with a steerable filter may be uniquely expressed in terms of direct and inverse scalar spherical harmonics transforms. The separation of variable technique sets the asymptotic complexity of the scalar transform to  $\mathcal{O}(L^3)$ . The specific use of equi-angular pixelizations allows to achieve the exactness of the algorithm, through a sampling theorem introduced by Driscoll and Healy for their fast scalar spherical harmonics transform. If the associated Legendre polynomials necessary for the transform are pre-calculated, the asymptotic complexity of the Driscoll and Healy transform on equi-angular grids drops to an optimized  $\mathcal{O}(L^2 \log^2 L)$ . We discuss the numerical implementations of the scalar spherical harmonics transforms on equi-angular pixelizations (SpharmonicKit package) as well as on Hierarchical Equal-Area iso-Latitude pixelizations (HEALPix package). A simple comparative analysis of the corresponding memory requirements, computation times, and numerical stability shows that both implementations of the directional correlation algorithm are easily accessible on a standard computer for resolutions well beyond  $L \simeq 10^3$ . Finally, we briefly recall an existing alternative  $\mathcal{O}(L^4)$  algorithm for the directional correlation, which may also be optimized to an  $\mathcal{O}(L^3)$  asymptotic complexity through the use of steerable filters. In § 5, we consider the algorithm in the perspective of the scale-space analysis of the CMB, through the directional correlation of the temperature  $T$ , and of the electric  $E$  and magnetic  $B$  polarization components. We illustrate the performance of our algorithm through the explicit computation of the wavelet coefficients of a simulated CMB temperature map with the second Gaussian derivative wavelet. A comparison of the results of the equi-angular and HEALPix implementations is proposed. The good precision of the two implementations is confirmed with a clear advantage though for the equi-angular approach which is theoretically exact. The computation times of directional correlation of maps of several megapixels are reduced from years to tens of seconds. We briefly conclude in § 6.

## 2. DIRECTIONAL CORRELATION

### 2.1. Definition

We define here explicitly the notions of directional and standard correlations.

Let the function  $F(\omega)$  and the filter  $\Psi(\omega)$  be square-integrable functions in  $L^2(S^2, d\Omega)$  on the unit sphere  $S^2$ . The point  $\omega$  is given in the spherical coordinates defined in the right-handed Cartesian coordinate system  $(o, o\hat{x}, o\hat{y}, o\hat{z})$  centered on the unit sphere as:  $\omega = (\theta, \varphi)$ . The angle  $\theta \in [0, \pi]$  is the polar angle, or co-latitude. The angle  $\varphi \in [0, 2\pi[$  is the azimuthal angle, or longitude. The invariant measure on the sphere reads  $d\Omega = d\cos\theta d\varphi$ . Recall that an axisymmetric filter is by definition invariant under rotation on itself. That is, when located at the North pole, an axisymmetric filter is defined by a function  $\Psi(\theta)$  independent of the azimuthal angle  $\varphi$ . Any non-axisymmetric filter is said to be directional, and is given as a general function  $\Psi(\theta, \varphi)$  in  $L^2(S^2, d\Omega)$ . The directional correlation is defined as the

scalar product between the function  $F$  and an arbitrary filter  $\Psi$  rotated on itself in a direction  $\chi \in [0, 2\pi[$ , and translated at any point  $\omega_0 = (\theta_0, \varphi_0)$  on the sphere. The Euler angles  $(\varphi_0, \theta_0, \chi)$  associated with a general rotation in three dimensions  $\rho \in SO(3)$  represent successive rotations by  $\chi$  around  $o\hat{z}$ ,  $\theta_0$  around  $o\hat{y}$ , and  $\varphi_0$  around  $o\hat{z}$ . These may also be interpreted in the reverse order as successive rotations by  $\varphi_0$  around  $o\hat{z}$ ,  $\theta_0$  around  $o\hat{y}$ , and  $\chi$  around  $o\hat{z}$ , where the axes  $o\hat{y}' \equiv o\hat{y}'(\varphi_0)$  and  $o\hat{z}'' \equiv o\hat{z}''(\varphi_0, \theta_0)$  are respectively obtained by the first and second rotations of the coordinate system by  $\varphi_0$  and  $\theta_0$  (Brink & Satchler 1993). The translations of the filter  $\Psi$  at  $\omega = (\theta_0, \varphi_0)$  are thus associated with the two first Euler angles  $\varphi_0$  around  $o\hat{z}$ ,  $\theta_0$  around  $o\hat{y}'$ . The rotations of the filter on itself in the plane tangent to the sphere at  $\omega = (\theta_0, \varphi_0)$  are rotations around  $o\hat{z}''$ , associated with the third Euler angle  $\chi$ . The affine transformations considered are therefore implemented through the action on the function  $\Psi$  of the operators  $R(\rho)$  associated with a rotation  $\rho = (\varphi_0, \theta_0, \chi)$  in  $SO(3)$ . These operators read, in the first Euler angles interpretation, as  $R(\rho) = R^z(\varphi_0)R^y(\theta_0)R^z(\chi) = R(\omega_0)R^z(\chi)$ . The rotation  $R\Psi$  reads  $[R(\rho)\Psi](\omega) = \Psi(R_\rho^{-1}\omega)$ , where  $R_\rho = R_{\varphi_0}^z R_{\theta_0}^y R_\chi^z = R_{\omega_0} R_\chi^z$  stands for the three-dimensional rotation matrix associated with  $\rho$ , acting on the coordinates  $\omega = (\theta, \varphi)$ . The result of the directional correlation thus explicitly gives a square-integrable function in  $L^2(SO(3), d\rho)$  on the rotation group, for the invariant measure  $d\rho = d\cos\theta_0 d\varphi_0 d\chi$ .

The directional correlation  $\langle R\Psi|F \rangle$  of the function  $F$  by the filter  $\Psi$  thus explicitly reads in  $L^2(SO(3), d\rho)$  as:

$$\langle R(\rho)\Psi|F \rangle = \int_{S^2} d\Omega \Psi^*(R_\rho^{-1}\omega) F(\omega). \quad (1)$$

The standard correlation  $\langle R_0\Psi|F \rangle$  of  $F$  by  $\Psi$ , is defined by the scalar product between the function  $F$  and the filter  $\Psi$  translated at any point  $\omega_0 = (\theta_0, \varphi_0)$  on the sphere, but for a fixed direction, *i.e.* a fixed value  $\chi = 0$ . The result of the standard correlation explicitly gives a square-integrable function in  $L^2(S^2, d\Omega)$  on the sphere:

$$\langle R(\omega_0)\Psi|F \rangle = \int_{S^2} d\Omega \Psi^*(R_{\omega_0}^{-1}\omega) F(\omega). \quad (2)$$

The notation  $R_0$  simply identifies a three-dimensional rotation with  $\chi = 0$ . It distinguishes the standard correlation  $\langle R_0\Psi|F \rangle$  from the directional correlation  $\langle R\Psi|F \rangle$  when the arguments are not specified. In the particular case of an axisymmetric filter, there is no dependence of the correlation in the filter rotation  $\chi$ . The directional correlation with an axisymmetric filter is therefore strictly equivalent to the standard correlation.

Notice that if  $\Psi$  is the specific dilation by  $a \in \mathbb{R}_+^*$  of a wavelet on the sphere,  $\Psi \rightarrow \Psi_a$ , the directional correlation identifies with the wavelet coefficient of the signal, at the corresponding scale:  $W_\Psi^F(\omega_0, \chi, a) = \langle R(\rho)\Psi_a|F \rangle$ , for  $\rho = (\varphi_0, \theta_0, \chi)$  (Wiaux et al. 2005). Let us finally remark that the correlation is also generically called convolution on the sphere (Wandelt & Górski 2001). We use a specific terminology to avoid any confusion with other definitions (Driscoll & Healy 1994; Healy et al. 2003).

## 2.2. A priori computation cost

The numerical computation cost associated with a naive discretization, or quadrature, of the relation (1) for the directional correlation of functions on the sphere may easily be estimated in the following way.

First, let  $N_p = (2L)^2$  represent the number of sampling points  $\omega$  in a given pixelization of the sphere. The quantity  $2L$  represents the mean number of sampling points in the position variables  $\theta$  and  $\varphi$ . A simple extrapolation of the Nyquist-Shannon theorem on the line intuitively associates  $L$  with the band limit, or maximum frequency, accessible in the ‘‘Fourier’’ indices conjugate to  $\theta$  and  $\varphi$  for the signals and filters considered. To an equivalent sampling on  $2L$  points in the direction  $\chi$  also corresponds a band limit  $L$  in the conjugate Fourier index.

Second, considering a simple discretization of the relation of directional correlation, each integration on  $\omega = (\theta, \varphi)$  on the sphere, a scalar product, has an asymptotic complexity  $\mathcal{O}(L^2)$ . The directional correlation is associated with the calculation of a scalar product for each discrete  $\rho = (\varphi_0, \theta_0, \chi)$  on  $SO(3)$ . The corresponding naive asymptotic complexity is therefore of order  $\mathcal{O}(L^5)$ .

Third, we consider fine samplings of several megapixels on the sphere associated with a band limit around  $L \simeq 10^3$ . In particular, present CMB experiments such as the WMAP mission provide all-sky maps of around three megapixels. For such a fine sampling, the typical computation times for  $(2L)^2$  multiplications and  $(2L)^2$  additions are of order of 0.03 seconds on a standard 2.2 GHz Intel Pentium Xeon CPU, for double-precision numbers. We take this value as a fair estimation of the computation time required for a scalar product in (1). Consequently, a unique  $\mathcal{O}(L^5)$  directional correlation would take several years at that band limit  $L \simeq 10^3$  on a single standard computer. Moreover, depending on the application, the directional correlation of multiple signals might be required. Typically, thousands of simulated signals are to be considered for a statistical (CMB) analysis.

In conclusion, the computation time for a simple  $\mathcal{O}(L^5)$  discretization of the relation for the directional correlation of functions on the sphere is absolutely unaffordable for fine samplings with a band limit around  $L \simeq 10^3$  in  $\theta$ ,  $\varphi$ , and  $\chi$ . This conclusion remains when the use of multiple computers is envisaged. It is even strongly reinforced in the perspective of a scale-space analysis on the sphere from finer pixelizations. In particular, the future all-sky CMB maps of the Planck mission will reach samplings of fifty megapixels, *i.e.*  $L \simeq 4 \times 10^3$ .

## 2.3. Directional correlation as a Wigner transform

We here discuss the decomposition of the directional correlation as an inverse Wigner  $D$ -functions transform on  $SO(3)$ .

First, we recall the decomposition of functions on  $S^2$  and  $SO(3)$  in standard scalar spherical harmonics and Wigner  $D$ -functions respectively. The standard scalar spherical harmonics  $Y_{lm}(\omega)$ , with  $l \in \mathbb{N}$ ,  $m \in \mathbb{Z}$ , and  $|m| \leq l$ , form an orthonormal basis for the decomposition of functions in  $L^2(S^2, d\Omega)$  on the sphere, with  $\omega = (\theta, \varphi)$  (Varshalovich et al. 1989). They are explicitly given in a factorized form in terms of the associated Legendre polynomials  $P_l^m(\cos\theta)$  and the complex exponentials  $e^{im\varphi}$  as

$$Y_{lm}(\theta, \varphi) = \left[ \frac{2l+1}{4\pi} \frac{(l-m)!}{(l+m)!} \right]^{1/2} P_l^m(\cos\theta) e^{im\varphi}. \quad (3)$$

This corresponds to the choice of Condon-Shortley phase  $(-1)^m$  for the spherical harmonics, ensuring the relation  $(-1)^m Y_{lm}^*(\omega) = Y_{l(-m)}(\omega)$ . This phase is here included in the definition of the associated Legendre polynomials (Abramowitz & Stegun 1965; Varshalovich et al. 1989). Another convention (Brink & Satchler 1993) explicitly transfers

it to the spherical harmonics. The orthonormality and completeness relations respectively read:

$$\int_{S^2} d\Omega Y_{lm}^*(\omega) Y_{l'm'}(\omega) = \delta_{ll'} \delta_{mm'}, \quad (4)$$

and

$$\sum_{l \in \mathbb{N}} \sum_{|m| \leq l} Y_{lm}^*(\omega') Y_{lm}(\omega) = \delta(\omega' - \omega), \quad (5)$$

with  $\delta(\omega' - \omega) = \delta(\cos \theta' - \cos \theta) \delta(\varphi' - \varphi)$ . Any function  $G(\omega)$  on the sphere is thus uniquely given as a linear combination of scalar spherical harmonics (inverse transform):

$$G(\omega) = \sum_{l \in \mathbb{N}} \sum_{|m| \leq l} \widehat{G}_{lm} Y_{lm}(\omega), \quad (6)$$

for the scalar spherical harmonics coefficients (direct transform)

$$\widehat{G}_{lm} = \int_{S^2} d\Omega Y_{lm}^*(\omega) G(\omega), \quad (7)$$

with  $|m| \leq l$ .

The Wigner  $D$ -functions  $D_{mn}^l(\rho)$ , for  $\rho = (\varphi, \theta, \chi) \in SO(3)$ , and with  $l \in \mathbb{N}$ ,  $m, n \in \mathbb{Z}$ , and  $|m|, |n| \leq l$ , are the matrix elements of the irreducible unitary representations of weight  $l$  of the rotation group  $SO(3)$ , in  $L^2(SO(3), d\rho)$ . By the Peter-Weyl theorem on compact groups, the matrix elements  $D_{mn}^{l*}$  also form an orthogonal basis in  $L^2(SO(3), d\rho)$  (Varshalovich et al. 1989). They are explicitly given in a factorized form in terms of the real Wigner  $d$ -functions  $d_{mn}^l(\theta)$  and the complex exponentials,  $e^{-im\varphi}$  and  $e^{-in\chi}$ , as

$$D_{mn}^l(\varphi, \theta, \chi) = e^{-im\varphi} d_{mn}^l(\theta) e^{-in\chi}. \quad (8)$$

The Wigner  $d$ -functions read

$$d_{mn}^l(\theta) = \sum_{t=C_1}^{C_2} \frac{(-1)^t [(l+m)!(l-m)!(l+n)!(l-n)!]^{1/2}}{(l+m-t)!(l-n-t)!t!(t+n-m)!} (\cos \theta/2)^{2l+m-2t} (\sin \theta/2)^{2t+n-m}, \quad (9)$$

with the summation bounds  $C_1 = \max(0, m-n)$  and  $C_2 = \min(l+m, l-n)$  defined to consider only factorials of positive integers. They satisfy various symmetry properties on their indices (Varshalovich et al. 1989). The orthogonality and completeness relations of the Wigner  $D$ -functions respectively read:

$$\int_{SO(3)} d\rho D_{mn}^l(\rho) D_{m'n'}^{l*}(\rho) = \frac{8\pi^2}{2l+1} \delta_{ll'} \delta_{mm'} \delta_{nn'}, \quad (10)$$

and

$$\sum_{l \in \mathbb{N}} \frac{2l+1}{8\pi^2} \sum_{|m|, |n| \leq l} D_{mn}^l(\rho') D_{mn}^{l*}(\rho) = \delta(\rho' - \rho), \quad (11)$$

with  $\delta(\rho' - \rho) = \delta(\varphi' - \varphi) \delta(\cos \theta' - \cos \theta) \delta(\chi' - \chi)$ . Any function  $G(\rho)$  in  $L^2(SO(3), d\rho)$  is thus uniquely given as a linear combination of Wigner  $D$ -functions (inverse transform):

$$G(\rho) = \sum_{l \in \mathbb{N}} \frac{2l+1}{8\pi^2} \sum_{|m|, |n| \leq l} \widehat{G}_{mn}^l D_{mn}^{l*}(\rho), \quad (12)$$

for the Wigner  $D$ -functions coefficients (direct transform)

$$\widehat{G}_{mn}^l = \int_{SO(3)} d\rho D_{mn}^l(\rho) G(\rho), \quad (13)$$

with  $|m|, |n| \leq l$ .

Second, we expose the decomposition of the directional correlation in Wigner  $D$ -functions. The Wigner  $D$ -functions coefficients  $\langle \widehat{R\Psi|F} \rangle_{mn}^l$  of the directional correlation  $\langle R(\rho)\Psi|F \rangle$  are given as the pointwise product of the scalar spherical harmonics coefficients  $\widehat{F}_{lm}$  and  $\widehat{\Psi}_{ln}^*$ . The following directional correlation relation indeed holds:

$$\langle R(\rho)\Psi|F \rangle = \sum_{l \in \mathbb{N}} \frac{2l+1}{8\pi^2} \sum_{|m|, |n| \leq l} \langle \widehat{R\Psi|F} \rangle_{mn}^l D_{mn}^{l*}(\rho), \quad (14)$$

with the Wigner  $D$ -functions coefficients on  $SO(3)$   $\langle \widehat{R\Psi|F} \rangle_{mn}^l$  given as

$$\langle \widehat{R\Psi|F} \rangle_{mn}^l = \frac{8\pi^2}{2l+1} \widehat{\Psi}_{ln}^* \widehat{F}_{lm}. \quad (15)$$

The derivation of this result goes as follows. The orthonormality of scalar spherical harmonics implies the following Plancherel relation  $\langle R\Psi|F \rangle = \sum_{l \in \mathbb{N}} \sum_{|m| \leq l} \widehat{R\Psi}_{lm}^* \widehat{F}_{lm}$ . The action of the operator  $R(\rho)$  on a function  $G(\omega)$  in  $L^2(S^2, d\Omega)$  on the sphere reads in terms of its scalar spherical harmonics coefficients and the Wigner  $D$ -functions as:  $[\widehat{R(\rho)G}]_{lm} = \sum_{|n| \leq l} D_{mn}^l(\rho) \widehat{G}_{ln}$ . Inserting this last relation for  $\Psi$  in the former Plancherel relation finally gives the result. In the particular case of an axisymmetric filter  $\Psi(\theta)$ , the above relation reduces to the following standard correlation relation:  $\langle \widehat{R_0\Psi|F} \rangle_{lm} = 2\pi \widehat{\Psi}_l^* \widehat{F}_{lm}$ , where  $\widehat{\Psi}_l$  stands for the Legendre coefficient of the filter.

### 3. FILTER STEERABILITY

#### 3.1. Definition

We here recall the notion of filter steerability on the sphere (Wiaux et al. 2005; Freeman & Adelson 1991; Simoncelli et al. 1992) and give explicit examples. A directional filter  $\Psi$  in  $L^2(S^2, d\Omega)$  on the sphere is steerable if any rotation by  $\chi \in [0, 2\pi[$  of the filter around itself  $R^\chi(\Psi)$  may be expressed as a linear combination of a finite number of basis filters  $\Psi_m$ :

$$[R^\chi(\Psi)](\omega) = \sum_{m=1}^M k_m(\chi) \Psi_m(\omega). \quad (16)$$

The weights  $k_m(\chi)$ , with  $1 \leq m \leq M$ , and  $M \in \mathbb{N}$ , are called interpolation functions. In particular cases, the basis filters may be specific rotations by angles  $\chi_m$  of the original filter:  $\Psi_m = R^{\chi_m}(\Psi)$ . Steerable filters have a non-zero angular width in the azimuthal angle  $\varphi$  which makes them sensitive to a whole range of directions and enables them to satisfy the relation (16). In the spherical harmonics space, this non-zero angular width corresponds to an azimuthal angular band limit  $N$  in the index  $n$  associated with the azimuthal variable  $\varphi$ :  $\widehat{\Psi}_{ln} = 0$  for  $|n| \geq N$ .

The inverse stereographic projection on the sphere of the  $N_d^{\text{th}}$  derivative in direction  $\hat{x}$  of radial functions on the plane (tangent at the North pole) are steerable filters. They may be rotated in terms of  $M = N_d + 1$  basis filters, and are band-limited in  $\varphi$  at  $N = N_d + 1$ . We give here the explicit examples of the normalized first and second Gaussian derivatives. A first derivative has a band limit  $N = 2$ , and only contains the indices  $n = \{\pm 1\}$ . It may be rotated in terms of two specific rotations at  $\chi = 0$  and  $\chi = \pi/2$ , corresponding to the inverse

projection of the first derivatives in directions  $\hat{x}$  and  $\hat{y}$ ,  $\Psi^{\partial_{\hat{x}}}$  and  $\Psi^{\partial_{\hat{y}}}$  respectively:

$$[R^{\hat{z}}(\chi)\Psi^{\partial_{\hat{x}}}] (\omega) = \Psi^{\partial_{\hat{x}}}(\omega) \cos \chi + \Psi^{\partial_{\hat{y}}}(\omega) \sin \chi. \quad (17)$$

The normalized first derivatives of a Gaussian in directions  $\hat{x}$  and  $\hat{y}$  read:

$$\begin{aligned} \Psi^{\partial_{\hat{x}}(\text{gauss})}(\theta, \varphi) &= \sqrt{\frac{8}{\pi}} \left(1 + \tan^2 \frac{\theta}{2}\right) e^{-2 \tan^2(\theta/2)} \tan \frac{\theta}{2} \cos \varphi \\ \Psi^{\partial_{\hat{y}}(\text{gauss})}(\theta, \varphi) &= \sqrt{\frac{8}{\pi}} \left(1 + \tan^2 \frac{\theta}{2}\right) e^{-2 \tan^2(\theta/2)} \tan \frac{\theta}{2} \sin \varphi. \end{aligned} \quad (18)$$

A second derivative has a band limit  $N = 3$ , and contains the frequencies  $n = \{0, \pm 2\}$ . It may be rotated in terms of three basis filters. It reads indeed in terms of the inverse projection of the second derivatives in directions  $\hat{x}$  and  $\hat{y}$ ,  $\Psi^{\partial_{\hat{x}}^2}$  and  $\Psi^{\partial_{\hat{y}}^2}$  respectively, and the cross derivative  $\Psi^{\partial_{\hat{x}}\partial_{\hat{y}}}$  as:

$$\begin{aligned} [R^{\hat{z}}(\chi)\Psi^{\partial_{\hat{x}}^2}] (\omega) &= \Psi^{\partial_{\hat{x}}^2}(\omega) \cos^2 \chi + \Psi^{\partial_{\hat{y}}^2}(\omega) \sin^2 \chi \\ &\quad + \Psi^{\partial_{\hat{x}}\partial_{\hat{y}}}(\omega) \sin 2\chi. \end{aligned} \quad (19)$$

The correctly normalized second derivatives of a Gaussian in directions  $\hat{x}$  and  $\hat{y}$  read:

$$\begin{aligned} \Psi^{\partial_{\hat{x}}^2(\text{gauss})}(\theta, \varphi) &= \sqrt{\frac{4}{3\pi}} \left(1 + \tan^2 \frac{\theta}{2}\right) e^{-2 \tan^2(\theta/2)} \\ &\quad \left(1 - 4 \tan^2 \frac{\theta}{2} \cos^2 \varphi\right) \\ \Psi^{\partial_{\hat{y}}^2(\text{gauss})}(\theta, \varphi) &= \sqrt{\frac{4}{3\pi}} \left(1 + \tan^2 \frac{\theta}{2}\right) e^{-2 \tan^2(\theta/2)} \\ &\quad \left(1 - 4 \tan^2 \frac{\theta}{2} \sin^2 \varphi\right) \\ \Psi^{\partial_{\hat{x}}\partial_{\hat{y}}(\text{gauss})}(\theta, \varphi) &= -\frac{4}{\sqrt{3\pi}} \left(1 + \tan^2 \frac{\theta}{2}\right) e^{-2 \tan^2(\theta/2)} \\ &\quad \left(\tan^2 \frac{\theta}{2} \sin 2\varphi\right). \end{aligned} \quad (20)$$

### 3.2. From directional to standard correlation

We here express the directional correlation of arbitrary signals with steerable filters in terms of standard correlations.

The relation of steerability (16) is obviously preserved by linear filtering. The directional correlation of a signal  $F$  by a steerable filter  $\Psi$  therefore satisfies the same steerability relation as the filter itself:

$$\langle R(\rho)\Psi|F \rangle = \sum_{m=1}^M k_m(\chi) \langle R(\omega_0)\Psi_m|F \rangle, \quad (21)$$

for  $\rho = (\varphi_0, \theta_0, \chi)$ , and  $\omega_0 = (\varphi_0, \theta_0)$ . The steerability therefore enables the computation of the directional correlation of a signal  $F$  with a steerable filter  $\Psi$  as a linear combination with known weights  $k_m(\chi)$ , of  $M$  standard correlations with the basis filters  $\Psi_m$ . For steerable filters with  $M \ll L$ , this quantity  $M$  disappears from asymptotic complexities calculations. In conclusion, the asymptotic complexity of the directional correlation with a steerable filter is reduced to the asymptotic complexity of a standard correlation, to which must be added the  $\mathcal{O}(L^3)$  operations required for the explicit computation of

the directional correlation through the relation (21). Already notice that the *a priori* computation cost associated with the discretization of the directional correlation integral (1) with a steerable filter is lowered from  $\mathcal{O}(L^5)$  to  $\mathcal{O}(L^4)$  through the calculation of standard correlation integrals (2) with the corresponding basis filters.

### 3.3. Standard correlation as a spin-weighted spherical harmonics transform

We here study the decomposition of the standard correlation as a sum of inverse spin-weighted spherical harmonics transforms on the sphere.

Let us first recall the notion of spin  $n$  function in  $L^2(S^2, d\Omega)$  on the sphere and the related decomposition in spin-weighted spherical harmonics of spin  $n$ . As defined in § 2, in the coordinate frame  $(o, o\hat{x}, o\hat{y}, o\hat{z})$ , the Euler angles  $(\varphi, \theta, \chi)$  associated with a general rotation in three dimensions may be interpreted as successive rotations by  $\varphi \in [0, 2\pi[$  around  $o\hat{z}$ ,  $\theta \in [0, \pi]$  around  $o\hat{y}'(\varphi)$ , and  $\chi \in [0, 2\pi[$  around  $o\hat{z}''(\varphi, \theta)$ . The local rotations of the basis vectors in the plane tangent to the sphere at  $\omega = (\theta, \varphi)$  are rotations around  $o\hat{z}''$ , associated with the third Euler angle  $\chi$ . Spin  $n$  functions on the sphere  ${}_nG(\omega)$ , with  $n \in \mathbb{Z}$ , are defined relatively to their behaviour under the corresponding right-handed rotations by  $\chi_0$  as (Newman & Penrose 1966; Goldberg et al. 1967; Carmeli 1969):

$${}_nG'(\omega) = e^{-in\chi_0} {}_nG(\omega). \quad (22)$$

We emphasize that the rotations considered are local transformations on the sphere around the axis  $o\hat{z}'' \equiv o\hat{z}''(\varphi, \theta)$ , affecting the coordinate  $\chi$  in the tangent plane independently at each point  $\omega = (\theta, \varphi)$ , according to  $\chi' = \chi - \chi_0$ . They are to be clearly distinguished from the global rotations  $R_{\chi}^{\hat{z}}$  associated with the alternative Euler angles interpretation, which affect the coordinates of the points  $\omega = (\theta, \varphi)$  on the sphere. Our sign convention in the exponential is coherent with the definition (23) here below for the spin-weighted spherical harmonics of spin  $n$ . It is opposite to the original definition (Newman & Penrose 1966), while equivalent to recent notations used in the context of the CMB analysis (Zaldarriaga & Seljak 1997; Challinor et al. 2000). Recalling the factorized form (8), spin functions are equivalently defined as the evaluation at  $\chi = 0$  of any function in  $L^2(SO(3), d\rho)$  resulting from an expansion for fixed index  $n$  in the Wigner  $D$ -functions  $D_{mn}^l(\varphi, \theta, \chi)$ . The functions  $D_{mn}^l(\varphi, \theta, 0)$  or  $D_{m(-n)}^{l*}(\varphi, \theta, 0)$  thus naturally define for each  $n$  an orthogonal basis for the expansion of spin  $n$  functions in  $L^2(S^2, d\Omega)$  on the sphere. Their normalization in  $L^2(S^2, d\Omega)$  defines the spin-weighted spherical harmonics of spin  $n$ :

$${}_nY_{lm}(\theta, \varphi) = (-1)^n \sqrt{\frac{2l+1}{4\pi}} D_{m(-n)}^{l*}(\varphi, \theta, 0), \quad (23)$$

with  $l \in \mathbb{N}$ ,  $l \geq |n|$ , and  $m \in \mathbb{Z}$ ,  $|m| \leq l$ . They are thus explicitly given in a factorized form in terms of the real Wigner  $d$ -functions  $d_{mn}^l(\theta)$  and the complex exponentials  $e^{im\varphi}$  as

$${}_nY_{lm}(\theta, \varphi) = (-1)^n \sqrt{\frac{2l+1}{4\pi}} d_{m(-n)}^l(\theta) e^{im\varphi}. \quad (24)$$

In particular, the symmetry properties of the Wigner  $d$ -functions imply the generalized relation  $(-1)^{n+m} {}_nY_{lm}^*(\omega) = {}_{-n}Y_{l(-m)}(\omega)$ . The spin 0 spherical harmonics explicitly identify with the standard scalar spherical harmonics:  ${}_0Y_{lm}(\omega) = Y_{lm}(\omega)$ , through the relation  $d_{m0}^l(\theta) = \left[\frac{(l-m)!}{(l+m)!}\right]^{1/2} P_l^m(\cos \theta)$ . The

orthonormality and completeness relations respectively read from relations (10) and (11), as

$$\int_{S^2} d\Omega {}_n Y_{lm}^*(\omega) {}_n Y_{l'm'}(\omega) = \delta_{ll'} \delta_{mm'}, \quad (25)$$

and

$$\sum_{l \in \mathbb{N}} \sum_{|m| \leq l} {}_n Y_{lm}^*(\omega') {}_n Y_{lm}(\omega) = \delta(\omega' - \omega), \quad (26)$$

with  $\delta(\omega' - \omega) = \delta(\cos \theta' - \cos \theta) \delta(\varphi' - \varphi)$ . Any spin  $n$  function  ${}_n G(\omega)$  on the sphere is thus uniquely given as a linear combination of spin  $n$  spherical harmonics (inverse transform):

$${}_n G(\omega) = \sum_{l \in \mathbb{N}} \sum_{|m| \leq l} {}_n \widehat{G}_{lm} {}_n Y_{lm}(\omega), \quad (27)$$

for the spin-weighted spherical harmonics coefficients (direct transform)

$${}_n \widehat{G}_{lm} = \int_{S^2} d\Omega {}_n Y_{lm}^*(\omega) G(\omega), \quad (28)$$

with  $l \geq |n|$ , and  $|m| \leq l$ .

The directional correlation at  $\chi = 0$  identifies with the standard correlation. From the above definitions, the relation (14) therefore leads to the following standard correlation relation on the sphere, expressed as a sum of inverse spin-weighted spherical harmonics transforms:

$$\langle R(\omega_0) \Psi | F \rangle = \sum_{n \in \mathbb{Z}} \left[ \sum_{l \geq |n|} \sum_{|m| \leq l} \langle \widehat{R_0 \Psi | F} \rangle_{lmn} {}_n Y_{lm}(\omega_0) \right], \quad (29)$$

with coefficients  $\langle \widehat{R_0 \Psi | F} \rangle_{lmn}$  explicitly defined as the pointwise products

$$\langle \widehat{R_0 \Psi | F} \rangle_{lmn} = (-1)^n \sqrt{\frac{4\pi}{2l+1}} \widehat{\Psi}_{l(-n)}^* \widehat{F}_{lm}. \quad (30)$$

For each  $n$ , these coefficients may be understood as spin-weighted spherical harmonics coefficients, but to be clearly distinguished from the spin-weighted spherical harmonics coefficients  ${}_n \langle \widehat{R_0 \Psi | F} \rangle_{lm}$  of the standard correlation, which do not find a pointwise product expression. Considering a real filter also implies the further simplification:  $(-1)^n \widehat{\Psi}_{l(-n)}^* = \widehat{\Psi}_{ln}$ .

#### 4. FAST ALGORITHM

##### 4.1. Algorithm and pixelization

In the following, we define the global structure of our algorithm and discuss pixelization choices.

In terms of the relations (29) and (30), the computation of the standard correlation of a signal  $F$  by a steerable filter  $\Psi$  may be performed with the following global structure: a direct scalar spherical harmonics transform of the signal and the filter,  $\widehat{\Psi}_{ln}$  and  $\widehat{F}_{lm}$ , a correlation in spherical harmonics space through a pointwise product, and a sum of inverse spin-weighted spherical harmonics transforms to obtain  $\langle R_0 \Psi | F \rangle$ .

We consider band-limited signals  $F$  at some band limit  $L$  on the sphere  $S^2$ , that is by definition  $\widehat{F}_{lm} = 0$  for  $l \geq L$ . From (30), the standard correlation of a band-limited signal  $F$  with a band limit  $L$  by an band-limited filter  $\Psi$  on the sphere is thus also band-limited, at the same band limit:  $\langle \widehat{R_0 \Psi | F} \rangle_{lmn} = 0$  for  $l \geq L$ . In order to achieve the limit frequency  $L$ , an extrapolation of the Nyquist-Shannon theorem on the line typically requires pixelizations with at least  $2L$  sampling points in the

polar angle  $\theta \in [0, \pi]$  and the azimuthal angle  $\varphi \in [0, 2\pi[$  on the sphere. In the context of the signal processing of the CMB maps, many pixelization schemes have been considered. We only quote here the HEALPix scheme (Hierarchical Equal Area iso-Latitude Pixelization) (Górski et al. 2005) notably used for the WMAP and Planck experiments, and the GLESP pixelization (Gauss-Legendre Sky Pixelization) (Doroshkevich et al. 2005a; Doroshkevich et al. 2005b). In particular, on a  $2L \times 2L$  equi-angular grid, a sampling result on the sphere states that the direct scalar and spin-weighted spherical harmonics coefficients of a band-limited function on the sphere may be computed exactly up to a band limit  $L$  as a finite weighted sum, *i.e.* a quadrature, of the sampled values of that function (Driscoll & Healy 1994; Kostelec et al. 2000). The weights are defined from the structure of the Legendre polynomials  $P_l(\cos \theta)$  on  $[0, \pi]$ . They are functions of  $\theta$ , but are independent of the azimuthal angle  $\varphi$  and of the spin  $n$  considered. The theoretical exactness of computation represents an advantage of equi-angular grids relative to other samplings. Inverse scalar and spin-weighted spherical harmonics transforms of band-limited functions can obviously be evaluated exactly on any grid as they are explicitly defined as finite sums from relations (6) and (27) with  $l < L$ .

##### 4.2. From spin-weighted to scalar spherical harmonics

We propose here an original expression of spin-weighted spherical harmonics as simple linear combinations of scalar spherical harmonics.

The spin  $n$  spherical harmonics may be related to spin  $n \pm 1$  spherical harmonics through the action of spin raising and lowering operators (Newman & Penrose 1966; Goldberg et al. 1967). The action of the spin raising  $\bar{\partial}$  and lowering  $\partial$  operators on a spin  $n$  function  ${}_n G$ , giving a spin  $n+1$  and  $n-1$  function respectively, is defined as

$$[\bar{\partial} {}_n G](\theta, \varphi) = \left[ -\sin^n \theta \left( \frac{\partial}{\partial \theta} + \frac{i}{\sin \theta} \frac{\partial}{\partial \varphi} \right) \sin^{-n} \theta {}_n G \right](\theta, \varphi), \quad (31)$$

and

$$[\partial {}_n G](\theta, \varphi) = \left[ -\sin^{-n} \theta \left( \frac{\partial}{\partial \theta} - \frac{i}{\sin \theta} \frac{\partial}{\partial \varphi} \right) \sin^n \theta {}_n G \right](\theta, \varphi), \quad (32)$$

with, under rotation by  $\chi_0$  in the tangent plane at  $\omega = (\theta, \varphi)$ :  $[\bar{\partial} {}_n G]'(\omega) = e^{-i(n+1)\chi_0} [\bar{\partial} {}_n G](\omega)$  and  $[\partial {}_n G]'(\omega) = e^{-i(n-1)\chi_0} [\partial {}_n G](\omega)$ . In these terms, the spin-weighted spherical harmonics of spin  $n$  are related to spin-weighted spherical harmonics of spin  $n+1$  and  $n-1$  through the following relations:

$$[\bar{\partial} {}_n Y_{lm}](\omega) = [(l-n)(l+n+1)]^{1/2} {}_{n+1} Y_{lm}(\omega), \quad (33)$$

and

$$[\partial {}_n Y_{lm}](\omega) = -[(l+n)(l-n+1)]^{1/2} {}_{n-1} Y_{lm}(\omega), \quad (34)$$

also implying

$$[\bar{\partial} \bar{\partial} {}_n Y_{lm}](\omega) = -(l-n)(l+n+1) {}_n Y_{lm}(\omega). \quad (35)$$

The corresponding direct relation between the spin-weighted spherical harmonics of spin  $n$  and scalar spherical harmonics reads:

$${}_n Y_{lm}(\omega) = \left[ \frac{(l-n)!}{(l+n)!} \right]^{1/2} [\bar{\partial}^n Y_{lm}](\omega), \quad (36)$$

for  $0 \leq n \leq l$ , and

$${}_n Y_{lm}(\omega) = \left[ \frac{(l+n)!}{(l-n)!} \right]^{1/2} (-1)^n [\bar{\delta}^{-n} Y_{lm}](\omega), \quad (37)$$

for  $-l \leq n \leq 0$ .

Beyond these standard relations, we establish a recurrence relation free of derivatives for spin-weighted spherical harmonics as follows. Derivative relations satisfied by the Wigner  $D$ -functions (Varshalovich et al. 1989) allow to exchange the derivative in  $\theta$  in (33) and (34) for simple linear combinations. This gives the spin  $n$  spherical harmonics  ${}_n Y_{lm}$  as a linear combination of the spin  $n \mp 1$  spherical harmonics  ${}_{n \mp 1} Y_{lm}$  and  ${}_{n \mp 1} Y_{(l-1)m}$ :

$${}_n Y_{lm}(\theta, \varphi) = \left( \frac{l \mp n + 1}{l \pm n} \right)^{1/2} \frac{m \mp l \cos \theta}{l \sin \theta} {}_{n \mp 1} Y_{lm}(\theta, \varphi) \pm \left[ \frac{2l+1}{2l-1} \frac{(l \pm n - 1)(l^2 - m^2)}{l \pm n} \right]^{1/2} \frac{1}{l \sin \theta} {}_{n \mp 1} Y_{(l-1)m}(\theta, \varphi), \quad (38)$$

under the convention that  ${}_n Y_{lm}$  is defined to be zero for  $l < \max(|m|, |n|)$ . Grouping terms through their  $1/\sin \theta$  or  $\cot \theta$  pre-factors on the sphere, one gets in compact form the following 2-terms relation:

$${}_n Y_{lm}(\theta, \varphi) = \left( \frac{\frac{m}{l} \alpha_{(ln)}^{\pm} \pm \beta_{(lmm)}^{\pm} S^{-1}}{\sin \theta} \mp \alpha_{(ln)}^{\pm} \cot \theta \right) {}_{n \mp 1} Y_{lm}(\theta, \varphi), \quad (39)$$

with  $\alpha_{(ln)}^{\pm} = \left( \frac{l \mp n + 1}{l \pm n} \right)^{1/2}$ , and  $\beta_{(lmm)}^{\pm} = \frac{1}{l} \left[ \frac{2l+1}{2l-1} \frac{(l \pm n - 1)(l^2 - m^2)}{l \pm n} \right]^{1/2}$ . The operators  $S^{\pm 1} : l \rightarrow l \pm 1$  define a one-unit shift in the index  $l$ :  $[S^{-1} {}_{n \mp 1} Y_{lm}](\omega) = {}_{n \mp 1} Y_{(l-1)m}(\omega)$ . By a simple  $|n|$ -steps recurrence, spin-weighted spherical harmonics may therefore be expressed as a  $2^{|n|}$ -terms linear combination of scalar spherical harmonics. The same relation between spin-weighted and scalar spherical harmonics may also be obtained from relations (36) and (37) and direct derivative relations for the associated Legendre polynomials (Abramowitz & Stegun 1965).

### 4.3. Detailed algorithmic structure from scalar spherical harmonics transforms

In the following, we discuss the detailed structure of the algorithm, which may essentially be decomposed in a combination of scalar spherical harmonics transforms, and study the corresponding asymptotic complexity.

From the recurrence (39), the inverse spin-weighted transforms of  $\langle \bar{R}_0 \Psi | F \rangle_{lmm}$  at each  $n$  required in the relation (29) for the standard correlation may be decomposed as a linear combination of inverse scalar spherical harmonics transforms. Hence, the complete standard correlation of a band-limited signal with a band-limited steerable filter essentially relies on direct and inverse scalar spherical harmonics transforms.

The *a priori* complexity associated with the naive computation of the direct scalar transform integral (7) in  $(\theta, \varphi)$  on the sphere through simple quadrature, for all  $(l, m)$  with  $|m| \leq l < L$ , or with the sum on  $(l, m)$  for all discrete points  $(\theta, \varphi)$  in the inverse scalar transform (6) is naturally of order  $\mathcal{O}(L^4)$ . The separation of variables (3) in the scalar spherical harmonics into the associated Legendre polynomials  $P_l^m(\cos \theta)$  and the complex exponentials  $e^{im\varphi}$  allows to compute direct and inverse scalar spherical harmonics transforms

as successive transforms in each of the variables  $\theta$  and  $\varphi$  in  $\mathcal{O}(L^3)$  operations. The application of the concept of separation of variables on the sphere only requires that the sampling in the polar angle  $\theta$  be independent of the azimuthal angle  $\varphi$ . This criterion is met for a large variety of pixelizations. We will consider the corresponding stable numerical implementations on HEALPix pixelizations (Górski et al. 2005)<sup>2</sup>. For a  $2L \times 2L$  equi-angular grid in  $(\theta, \varphi)$  on the sphere, a further optimized algorithm exists which is due to Driscoll and Healy (Driscoll & Healy 1994). It explicitly takes advantage of a recurrence relation in  $l$  on the associated Legendre polynomials  $P_l^m(\cos \theta)$  to compute the associated Legendre transforms in  $\mathcal{O}(L \log_2^2 L)$  operations for each  $m$ . The Fourier transforms in  $e^{im\varphi}$  are computed in  $\mathcal{O}(L \log_2 L)$  operations for each  $\theta$  through standard Cooley-Tukey fast Fourier transforms. In these terms, the direct and inverse scalar spherical harmonics transforms of a band-limited function of band limit  $L$  on the sphere are computed in  $\mathcal{O}(L^2 \log_2^2 L)$  operations. Moreover, contrarily to the HEALPix implementation, the algorithm is theoretically exact. The exactness of the direct transform relies on the specific choice of weighting functions only depending on  $\theta$ , as required by the sampling result on equi-angular grids on the sphere. Again, the exactness of the evaluation of the inverse scalar spherical harmonics transform of a band-limited function relies on the fact that is expressed as the simple finite sum (6) with  $l < L$ . We will consider the corresponding stable numerical implementations of the SpharmonicKit package (Healy et al. 2003; Healy et al. 2004)<sup>3</sup>. As detailed in § 4.4, if high resolutions are to be considered ( $L > 1024$ ), the associated Legendre polynomials are not pre-calculate in order to avoid a too large RAM memory consumption. They must be computed on the fly and the corresponding  $\mathcal{O}(L^3)$  time consumption is included in the global asymptotic complexity for the spherical harmonics transform. Both the  $\mathcal{O}(L^3)$  HEALPix implementation and the  $\mathcal{O}(L^2 \log_2^2 L)$  SpharmonicKit implementation therefore effectively have the same global  $\mathcal{O}(L^3)$  asymptotic complexity when the calculation of the associated Legendre polynomials is considered.

Each inverse spin-weighted transform required in (29) *a priori* reads as  $2^{|n|}$ -terms linear combination from the recurrence (39). But these terms may be grouped in  $|n|+1$  inverse scalar spherical harmonics transforms with pre-factors  $\cot^p \theta / \sin^q \theta$  for  $p, q \in \mathbb{N}$  and  $p+q = |n|$ . In addition, for each  $p$  and  $q$  with  $p+q = |n|$ , the coefficients for the spins  $n$  and  $-n$  may be grouped before applying the corresponding inverse scalar spherical harmonics transform. This allows to consider only spin-weighted transforms for positive spins and correspondingly further reduces the number of scalar transforms required for the standard correlation.

Notice that another recurrence relation might be substituted to (39) for the treatment of the inverse spin-weighted transforms through inverse scalar transforms. This other relation explicitly relates  ${}_n Y_{lm}$  with  ${}_{n \mp 1} Y_{lm}$ ,  ${}_{n \mp 1} Y_{(l-1)m}$ , and  ${}_{n \mp 1} Y_{(l+1)m}$  (Varshalovich et al. 1989; Kostelec et al. 2000). The term  ${}_{n \mp 1} Y_{(l+1)m}(\omega) = [S^{+1} {}_{n \mp 1} Y_{lm}](\omega)$  actually raises the band limit of the associated scalar functions to be analyzed to  $L + |n|$  after the  $|n|$ -steps recurrence leading from spin-weighted to scalar spherical harmonics, with  $|n| < L$ . From a practical

<sup>2</sup> See [healpix.jpl.nasa.gov](http://healpix.jpl.nasa.gov) for documentation and algorithm implementation (HEALPix2.1 software).

<sup>3</sup> See [www.cs.dartmouth.edu/~geelong/sphere/](http://www.cs.dartmouth.edu/~geelong/sphere/) for unpublished documentation and algorithm implementation (SpharmonicKit package).

point of view, in a HEALPix scheme for a fixed resolution, this will reduce the numerical precision of computation, as the implementation is known to make larger errors at higher  $l$ 's. On  $2L \times 2L$  equi-angular grids, the SpharmonicKit package is technically limited to consider coefficients up to  $L$ , and numerical errors will occur due to the absence of consideration of the coefficients between  $L$  and  $L + |n|$ . No such issue occurs from relation (39) which preserves the band limit  $L$  to be considered for the associated scalar functions.

In that context, let us analyze the overall asymptotic complexity of the standard correlation algorithm proposed. We consider steerable filters with low azimuthal angular band limit  $N \ll L$ , which constrain the maximum spin value to  $|n| < N$ . Typically  $N = 2$  for a first Gaussian derivative, and  $N = 3$  for a second Gaussian derivative. The index  $n$  therefore decouples from any asymptotic complexity contribution. The required direct and inverse scalar transforms set the overall asymptotic complexity of the standard correlation to  $\mathcal{O}(L^3)$  (and even to  $\mathcal{O}(L^2 \log_2^2 L)$  on equi-angular grids if the associated Legendre polynomials were to be pre-calculated). The asymptotic complexities of additional contributions to the algorithm are of order  $\mathcal{O}(L^2)$  and therefore negligible. First, the pointwise product (30) required after the direct transforms of the signal and the filter is indeed of order  $\mathcal{O}(L^2)$ . Second, the grouping of the  $2^{|n|}$  terms in the recurrence for each inverse spin-weighted spherical harmonics transform at spin  $n$ , as  $|n| + 1$  terms on which inverse scalar spherical harmonics are computed, contribute to the asymptotic complexity as  $2^{|n|} \times \mathcal{O}(L^2)$ . This contribution is also negligible for a first or second Gaussian derivative filter.

In summary, our algorithm for the standard correlation of a band-limited signal with a band-limited steerable filter is structured as follows, with related asymptotic complexities:

- Direct scalar spherical harmonics transforms,  $\widehat{\Psi}_{lm}$  and  $\widehat{F}_{lm}$ :  $\mathcal{O}(L^3)$  on all pixelizations ( $\mathcal{O}(L^2 \log_2^2 L)$  on an equi-angular grid if the associated Legendre polynomials are pre-calculated).
- Correlation  $\langle \widehat{R}_0 \widehat{\Psi} | \widehat{F} \rangle_{lmn}$  in spherical harmonics space:  $\mathcal{O}(L^2)$  through (30).
- Sum of inverse scalar spherical harmonics transforms to obtain  $\langle \widehat{R}_0 \widehat{\Psi} | \widehat{F} \rangle$  through (29) and (39):  $\mathcal{O}(L^3)$  on all pixelizations ( $\mathcal{O}(L^2 \log_2^2 L)$  on an equi-angular grid if the associated Legendre polynomials are pre-calculated).

Let us finally notice that the reduction of complexity to  $\mathcal{O}(L^2 \log_2^2 L)$  thanks to the use of an equi-angular grid beyond the calculation of the associated Legendre polynomials provides anyway an asymptotic reduction of the overall computation times for the corresponding correlation. It is therefore already of interest only in that respect. But the explicit calculation of the directional correlation from the relation (21) in terms of the computed standard correlations requires an additional  $\mathcal{O}(L^3)$  operation. However, we emphasize that all the information for the directional correlation of a signal with a steerable filter is already contained in the standard correlations with its basis filters. In many applications the explicit computation of the directional correlation through the relation (21) is not required. The interest may reside in the computation of the values of the directional correlation in a

small number of specific directions  $\chi_i$  at each point  $\omega_0$  on the sphere. One may also want to determine the direction  $\chi$  at each point  $\omega_0$  which maximizes the value of the directional correlation. In (Wiaux et al. 2005), this last application is illustrated in the perspective of the detection of the precise direction of local features in the CMB temperature and polarization anisotropies, through a steerable wavelet analysis. These features may represent potential signatures of fundamental non-Gaussianity or statistical anisotropy, or foreground emissions. The overall computation times for such a directional analysis are only driven by the asymptotic complexity of the standard correlations.

#### 4.4. Equi-angular and HEALPix implementations

We concisely compare the numerical SpharmonicKit and HEALPix packages for the scalar spherical harmonics transforms, in terms of memory requirements, computations times, and numerical stability. Those properties of the scalar spherical harmonics transforms implementations characterize the overall standard correlation implementations themselves. We also comment on the issue of the change of the pixelization on which the data are sampled, considering equi-angular and HEALPix grids.

Calculations are performed on a 2.20 GHz Intel Pentium Xeon CPU with 2 Gb of RAM memory. Random real test-signals are considered, with band limits  $L \in \{128, 256, 512, 1024\}$ . Without loss of generality, these real test-signals are defined through their scalar spherical harmonics coefficients  $\widehat{G}_{lm}$  with  $|m| \leq l < L$ , with independent real and imaginary parts uniformly distributed in the interval  $[-1, +1]$ . The reality condition  $\widehat{G}_{l(-m)} = (-1)^m \widehat{G}_{lm}^*$  obviously reduces computation times by a factor two relative to generic complex signals. The inverse and direct scalar spherical harmonics transforms are successively computed, giving numerical coefficients  $\widehat{H}_{lm}$ . The SpharmonicKit implementation is coded in C. The corresponding inverse transform is computed on  $2L \times 2L$  equi-angular pixelizations. For  $L = 1024$ , this corresponds to maps with  $N_{pix} = 4194304$  pixels. The direct transform is then recomputed exactly, *i.e.* to the computer's numerical precision, up to the band limit  $L$ . The HEALPix implementation considered is coded in Fortran90. The corresponding inverse transform is computed with a resolution identified by the parameter  $N_{side} = L/2$ , identifying maps with  $N_{pix} = 12N_{side}^2$  equal-area pixels. For  $L = 1024$ , the value  $N_{side} = 512$  defines maps with  $N_{pix} = 3145728$  pixels. The direct transform is then recomputed with a very good accuracy up to  $L = 2N_{side}$ .

RAM memory requirements for the scalar transforms are as follows. If the required associated Legendre polynomials  $P_l^m(\cos \theta)$  are pre-calculated once for all values of  $l$ ,  $\theta$ , and  $m$ , and stored in RAM memory, the number of real values of associated Legendre polynomials  $P_l^m(\cos \theta)$  stored in RAM memory for all  $l$ ,  $\theta$ , and  $m$  is of order  $\mathcal{O}(L^3)$ . The overall memory requirements allowing both direct and inverse transforms are still easily accessible but already higher than 1 Gb for  $L = 1024$ , for double-precision numbers. The pre-calculation computation time itself is of order  $\mathcal{O}(L^3)$  through the use of a recurrence relation in  $l$  on the associated Legendre polynomials. As a pre-calculation, the corresponding time consumption is not to be taken into account in the reported computation times, which consequently remain of order  $\mathcal{O}(L^2 \log_2^2 L)$  and  $\mathcal{O}(L^3)$  in the SpharmonicKit and the HEALPix implementations respectively. However, the corre-



sponding memory requirements rapidly become unaffordable for resolutions higher than  $L = 1024$ , such as the resolution expected for the Planck experiment. We therefore chose the SpharmonicKit and HEALPix implementations for which the required associated Legendre polynomials  $P_l^m(\cos\theta)$  are calculated on the fly, and stored in RAM memory for all values of  $l$  and  $\theta$ , but for only one value of  $m$  at the time. The reported computation times therefore inevitably include the  $\mathcal{O}(L^3)$  calculation of the Legendre polynomials, to be added to the remaining  $\mathcal{O}(L^2 \log^2 L)$  and  $\mathcal{O}(L^3)$  terms in the SpharmonicKit and the HEALPix implementations respectively. Both implementations effectively acquire the same global  $\mathcal{O}(L^3)$  asymptotic complexity. For fixed  $m$ , the number of real values  $P_l^m(\cos\theta)$  stored in RAM memory for all values of  $l$  and  $\theta$  is  $\mathcal{O}(L^2)$ . For the SpharmonicKit and HEALPix implementations, the overall memory requirements allowing both direct and inverse transforms are respectively of order  $1.3 \times 10^2$  Mb and  $4.6 \times 10^1$  Mb for  $L = 1024$ , for double-precision numbers. They are therefore significantly lower than the corresponding values when the associated Legendre polynomials are pre-calculated, and Planck-type resolutions are easily affordable.

The related computation times associated with these global  $\mathcal{O}(L^3)$  SpharmonicKit and HEALPix implementations for the inverse and direct transforms are given in Table 1. They are averages over 5 random band-limited real test-signals. They are of the order of tens of seconds at  $L = 1024$  both for the SpharmonicKit and the HEALPix implementations, in rough agreement with our previous intuitive estimation that an  $\mathcal{O}(L^2)$  operation requires 0.03 seconds on our standard computer. For the SpharmonicKit implementation, computation times evolve from  $1.0 \times 10^{-1}$  seconds for  $L = 128$  to  $4.6 \times 10^1$  seconds for  $L = 1024$ . For the HEALPix implementation, notice that an iterative scheme can be used for the direct transform, in order to enhance the accuracy of the calculation. After several iterations, the process converges towards a limit precision, which however never reaches the precision of the SpharmonicKit approach. For zero iteration ( $i = 0$ ), computation times evolve from  $4.8 \times 10^{-2}$  seconds for  $L = 128$  to  $1.5 \times 10^1$  seconds for  $L = 1024$ . The HEALPix implementation with a unique iteration is therefore slightly more rapid than the SpharmonicKit one, at least up to the band limit  $L = 1024$ . Computation times grow significantly with the number  $i$  of iterations used. For one iteration ( $i = 1$ ), the computation times for the direct transform are already bigger than for the SpharmonicKit implementation. They evolve from  $2.7 \times 10^{-1}$  seconds for  $L = 128$  to  $7.8 \times 10^1$  seconds for  $L = 1024$ .

The relative maximum error on the coefficients associated with the scalar spherical harmonics transforms is defined as  $\max_{l,m} |(\hat{G}_{lm} - \hat{H}_{lm}) / \hat{G}_{lm}|$ , where  $|\cdot|$  here denotes the complex norm. The relative root mean square numerical error is defined as the ratio of the  $L^2$ -norm of  $G-H$  and  $G$ , that is through the Plancherel relation:  $(\sum_{l,m} |\hat{G}_{lm} - \hat{H}_{lm}|^2 / \sum_{l,m} |\hat{G}_{lm}|^2)^{1/2}$ . The numerical errors given in Table 2 are averages for transforms over 5 random band-limited real test-signals. For the SpharmonicKit implementation, errors are extremely small as expected from the theoretical exactness of the algorithm. Relative maximum errors on the coefficients and relative root mean square errors are indeed bounded by  $1.8 \times 10^{-7}$  and  $7.5 \times 10^{-10}$  respectively, up to  $L = 1024$ . For the HEALPix implementation with zero iteration ( $i = 0$ ), the relative maximum errors on the coefficients can reach  $2.9 \times 10^1$ ,

TABLE 1  
SCALAR TRANSFORMS COMPUTATION TIMES

	Time $L = 128$ (sec)	Time $L = 256$ (sec)	Time $L = 512$ (sec)	Time $L = 1024$ (sec)
Spharmonic-Kit	1.0e-01	6.8e-01	5.2e+00	4.2e+01
HEALPix2.1 ( $i = 0$ )	4.8e-02	3.0e-01	2.0e+00	1.5e+01
HEALPix2.1 ( $i = 1$ )	2.7e-01	1.7e+00	1.1e+01	7.8e+01

NOTE. — Computation times for the SpharmonicKit and HEALPix2.1 implementations of the scalar spherical harmonics transforms, measured on a 2.20 GHz Intel Pentium Xeon CPU with 2 Gb of RAM memory. Times associated with the direct transform are listed above corresponding times for the inverse transform. The HEALPix2.1 direct transforms are reported both at  $i = 0$  and  $i = 1$  iteration.

TABLE 2  
SCALAR TRANSFORMS ERROR ANALYSIS

	Error $L = 128$	Error $L = 256$	Error $L = 512$	Error $L = 1024$
Spharmonic-Kit	3.3e-11	9.4e-11	2.6e-10	7.5e-10
HEALPix2.1 ( $i = 0$ )	7.0e-03	4.8e-03	3.5e-03	2.4e-03
HEALPix2.1 ( $i = 1$ )	2.7e-04	1.8e-04	1.4e-04	9.2e-05

NOTE. — Errors for the SpharmonicKit and HEALPix2.1 implementations of the scalar spherical harmonics transforms, measured on a 2.20 GHz Intel Pentium Xeon CPU with 2 Gb of RAM memory. Relative root mean square errors after inverse and direct transforms are listed above the corresponding relative maximum errors on the coefficients. HEALPix2.1 results are reported both at  $i = 0$  and  $i = 1$  iteration.

up to  $L = 1024$ . But the relative root mean square errors are bounded by  $7.0 \times 10^{-3}$ , up to  $L = 1024$ , which ensures the global numerical precision of the implementation. This already illustrates the numerical stability of the HEALPix implementation at the 0.7 % level, which however remains a much lower precision than with the SpharmonicKit implementation. The use of the iterative scheme for the computation of the direct transform allows to reach a better accuracy, at the price of a bigger time consumption. For the HEALPix implementation with one iteration ( $i = 1$ ), the relative maximum errors on the coefficients and relative root mean square errors are then bounded by 1.1 and  $2.7 \times 10^{-4}$  respectively, up to  $L = 1024$ , therefore achieving a numerical stability at the 0.027 % level.

Let us emphasize that the conclusions of this comparison of memory requirements, computation times, and numerical stability remain for the equi-angular and HEALPix implementations of our standard correlation algorithm. Indeed, the overall computation is strictly driven by the SpharmonicKit and HEALPix implementations of the scalar spherical harmonics transforms respectively.

We finally briefly comment on the issue of changing the pixelization on which the signal is defined, from HEALPix to equi-angular, or conversely. A specific choice of pixelization might be preferred for some analyses. The above results confirm the very good precision with which both implementations, with resolution  $N_{side} = L/2$  for HEALPix and on  $2L \times 2L$  equi-angular grids for SpharmonicKit, can calculate the direct and inverse transforms of a signal up to the band limit  $L$ . Consequently, a change of pixelization may be performed safely

by first computing the spherical harmonics coefficients of the signal by direct transform from one pixelization, and second operate an inverse transform on the alternative pixelization. The numerical precision of such an operation is obviously limited by the transform with the lowest precision, *i.e.* the HEALPix transform.

Notice however that any spectral or directional correlation analysis only uses the spherical harmonics coefficients of the signal. In that perspective, the question of pixelization change makes no sense. The initial pixelization on which the signal is defined does not constrain such analyses as both the HEALPix and SpharmonicKit implementations allow a precise calculation of the spherical harmonics coefficients of the signal. But the better numerical precision and lower computation times of the SpharmonicKit transform can really materialize if the data are originally sampled on equi-angular grids. Such a possibility must be evaluated for each application independently. The question can notably be raised for CMB experiments such as WMAP and Planck, which currently use HEALPix grids (Górski et al. 2005).

#### 4.5. Existing alternative procedure and optimization with steerable filters

For completeness of the discussion, we briefly expose an existing alternative algorithm for the directional correlation, based on the factorization of the rotation operators  $R(\rho)$  on functions in  $L^2(\mathcal{S}^2, d\Omega)$  on the sphere as (Risbo 1996; Wandelt & Górski 2001)

$$R(\varphi_0, \theta_0, \chi) = R\left(\varphi_0 - \frac{\pi}{2}, -\frac{\pi}{2}, \theta_0\right) R\left(0, \frac{\pi}{2}, \chi + \frac{\pi}{2}\right). \quad (40)$$

The directional correlation relation (14) and the expression (8) of the Wigner  $D$ -functions, matrix elements of the operators  $R(\rho)$ , therefore give an alternative expression for the directional correlation of arbitrary signals  $F$  and (non-steerable) filters  $\Psi$  on the sphere. We get indeed

$$\langle R(\rho) \Psi | F \rangle = \sum_{m, m', n \in \mathbb{Z}} \langle \widehat{R\Psi} | F \rangle_{mm'n} e^{i(m\varphi_0 + m'\theta_0 + n\chi)}, \quad (41)$$

with the Fourier coefficients on the three-torus  $\langle \widehat{R\Psi} | F \rangle_{mm'n}$  given by

$$\langle \widehat{R\Psi} | F \rangle_{mm'n} = e^{i(n-m)\pi/2} \sum_{l \geq C} d_{m'm}^l \left(\frac{\pi}{2}\right) d_{m'n}^l \left(\frac{\pi}{2}\right) \widehat{\Psi}_{ln} \widehat{F}_{lm}, \quad (42)$$

where  $C = \max(|m|, |m'|, |n|)$ , and with the symmetry relation  $d_{m'm}^l(\theta) = d_{m'm}^l(-\theta)$  (Varshalovich et al. 1989). For a band-limited signal  $F$  with band limit  $L$  on the sphere one has  $|m|, |m'|, |n| \leq l < L$ . In these terms, the directional correlation algorithm implemented through the factorization of rotations is structured as follows, with related asymptotic complexities:

- Direct scalar spherical harmonics transforms,  $\widehat{\Psi}_{ln}$  and  $\widehat{F}_{lm}$ :  $\mathcal{O}(L^3)$  on all pixelizations ( $\mathcal{O}(L^2 \log_2^2 L)$  on an equi-angular grid if the associated Legendre polynomials are pre-calculated).
- Correlation  $\langle \widehat{R\Psi} | F \rangle_{mm'n}$  in spherical harmonics space:  $\mathcal{O}(L^4)$  through (42).
- Inverse Fourier transform  $\langle R\Psi | F \rangle$  on the three-torus in  $(\theta_0, \varphi_0)$ :  $\mathcal{O}(L^3 \log_2 L)$  on an equi-angular grid by the use of the standard Cooley-Tukey fast Fourier transform algorithm, while  $\mathcal{O}(L^4)$  on HEALPix and other pixelizations.

The overall asymptotic complexity is therefore of order  $\mathcal{O}(L^4)$  independently of the pixelization, due to the correlation in spherical harmonics space.

Let us reconsider our first naive estimation of the computation times for the directional correlation on maps of several megapixels on the sphere. For  $L \simeq 10^3$ , an  $\mathcal{O}(L^4)$  algorithm already greatly reduces computation times from years down to days on a single standard computer. However, if a large number of signals have to be considered, say thousands of simulations, this remains hardly affordable even through the use of multiple computers.

Our algorithm achieves an  $\mathcal{O}(L^3)$  asymptotic complexity for the standard or directional correlation with steerable filters, and even an  $\mathcal{O}(L^2 \log_2^2 L)$  asymptotic complexity on equi-angular grids if the associated Legendre polynomials are pre-calculated. The algorithm described here using the factorization of rotations can also achieve an  $\mathcal{O}(L^3)$  complexity for the standard or directional correlation, if steerable filters are considered. Indeed, for a steerable filter  $\Psi$  with an azimuthal band limit  $N$ , the index  $n$  decouples from asymptotic complexity counts:  $|n| < N \ll L$ . But the corresponding structure does not allow any reduction to  $\mathcal{O}(L^2 \log_2^2 L)$ , as it clearly appears from relation (42).

Notice that the first proposal for the directional wavelet analysis of the CMB (McEwen et al. 2005a; McEwen et al. 2005b) was based on the presently discussed algorithm using the factorization of rotations. Instead of considering steerable wavelet filters, a much less precise sampling in  $P$  points in the direction  $\chi$  was defined, with  $P \ll L$ , typically reducing the precision in the directional analysis from  $\Delta\chi = 2\pi/L$  to  $\Delta\chi = 2\pi/P$ . This also artificially applies a band limit in the related Fourier index  $n$ :  $|n| < P$ . Technically, the asymptotic complexity of directional correlation is thus reduced like if a steerable filter with an azimuthal band limit  $P$  was considered. However, this is by no means an answer to the problem of the directional correlation of band-limited signals on the sphere if one requires the same high precision ( $P \simeq L$ ) in the analysis of local directions as for the position of features on the sphere. In that perspective, the use of steerable filters is essential. As discussed in (Wiaux et al. 2005), the theoretical angular resolution power of a steerable filter is infinite in the sense that, around each point of the signal, it can resolve exactly the direction of local features with a pre-defined morphology. It therefore makes complete sense to define a precise sampling in the analysis of local directions ( $P \simeq L$ ). If needed, the explicit calculation of the directional correlation for all sampled values of  $\chi$  therefore requires (see relation (21)) the additional  $\mathcal{O}(P \times L^2) \simeq \mathcal{O}(L^3)$  operation quoted in subsection 4.3. Obviously, the resolution of the angular morphology itself of a local feature is limited by the non-zero angular width of the steerable filter, *i.e.* its angular band limit  $N$  in the index  $n$  associated with the azimuthal angle  $\varphi$  when the filter is located at the North pole.

## 5. APPLICATION TO THE CMB SCALE-SPACE ANALYSIS

### 5.1. Temperature and polarization

The CMB radiation is completely described in terms of the observable temperature  $T$  and linear polarization  $Q$  and  $U$  Stokes parameters (Seljak & Zaldarriaga 1997; Zaldarriaga & Seljak 1997; Kosowsky 1996; Kamionkowski et al. 1997a; Kamionkowski et al. 1997b; Hu & White 1997). On the

one hand, the temperature is a scalar function on the sphere, *i.e.* invariant under local rotations in the plane tangent to the sphere at each point. It is also invariant under global inversion of the three-dimensional coordinates. On the other hand, the  $Q$  and  $U$  Stokes parameters are not invariant, but transform as the components of a transverse, symmetric, and traceless rank 2 tensor on the sphere, and respectively have even and odd parities under global inversion. Stated in other words, the combinations  $Q \pm iU$  are spin  $\pm 2$  functions on the sphere, and transform in one another under global inversion. In this context, the directional correlation of the temperature field with a scalar filter is invariant under the considered coordinates transformations. The directional correlations of the linear polarization parameters  $Q$  and  $U$  with a scalar filter are obviously not invariant, but transform in one another just as  $Q$  and  $U$ . A physical analysis will require the definition of invariant quantities. In that respect, the linear polarization of the CMB is equivalently defined by its electric  $E$  and magnetic  $B$  components, uniquely defined in terms of  $Q$  and  $U$ . These two polarization components are scalar functions on the sphere and also respectively have even and odd parities under global inversion. In this context, the statistics of a Gaussian and stationary CMB signal is completely described by the four invariant temperature ( $TT$ ), polarization ( $EE$  and  $BB$ ), and cross-correlation ( $TE$ ) angular power spectra. In the same idea, the complete scale-space analysis of the CMB data through directional correlation on the sphere will therefore rely the directional correlation of the scalar temperature  $T$ , and the scalar polarization components  $E$  and  $B$ , with an arbitrary scalar filter.

From the numerical point of view,  $E$  and  $B$  are related to the observables  $Q$  and  $U$  through derivative relations. It is consequently not possible to transform the experimental  $Q$  and  $U$  maps in scalar  $E$  and  $B$  maps from their basic definitions. However, the scalar spherical harmonics coefficients  $\hat{E}_{lm}$  and  $\hat{B}_{lm}$  are explicitly given as simple linear combinations of the spin  $\pm 2$  spherical harmonics coefficients  ${}_{\pm 2}(\hat{Q} \pm i\hat{U})_{lm}$ . From the recurrence relation (39), these spin  $n = \pm 2$  spherical harmonics coefficients may be computed as linear combinations of  $|n| + 1 = 3$  scalar spherical harmonics coefficients. The direct scalar spherical harmonics transforms of  $E$  and  $B$  can therefore be obtained from the experimental  $Q$  and  $U$  maps with the same asymptotic complexity as the direct scalar spherical harmonics transform of an experimental  $T$  map. From that stage, the remaining part of the detailed algorithmic structure proposed in § 4.3 can be applied identically to  $\hat{E}_{lm}$ ,  $\hat{B}_{lm}$ , or  $\hat{T}_{lm}$ . In summary, our algorithm can be applied both for the directional correlation of temperature and polarization CMB maps with steerable filters. The overall asymptotic complexity for the analysis of polarization maps remains  $\mathcal{O}(L^3)$  on all pixelizations ( $\mathcal{O}(L^2 \log^2 L)$  on an equi-angular grid if the associated Legendre polynomials are pre-calculated).

### 5.2. Numerical illustration

As an illustration we apply our algorithm to the computation of the wavelet coefficients of a temperature map with a second Gaussian derivative wavelet. A CMB temperature map is simulated both in the equi-angular and HEALPix pixelizations, from the angular power spectrum which best fits the three-year WMAP data. A comparison of the implementations of our algorithm on the two grids is proposed both in terms of computation times, and precision of analysis.

First, we produce a simulated CMB temperature map both

on equi-angular and HEALPix pixelizations in the following way. We define scalar spherical harmonics coefficients  $\hat{T}_{lm}$  from a Gaussian distribution with zero mean and a variance given by the temperature angular power spectrum  $C_l^{TT}$  which best fits the three-year WMAP data (Spergel et al. 2006), up to a band limit  $L = 1024$ . The spectrum  $C_l^{TT}$  was computed with CMBFAST<sup>4</sup>. Two real CMB temperature maps are then produced by inverse scalar spherical harmonics transforms of these coefficients, on a  $2L \times 2L$  equi-angular grid with the SpharmonicKit, and with a resolution  $N_{side} = L/2$  for the HEALPix pixelization.

Second, we apply our algorithm to produce the directional correlation of each map with a second Gaussian derivative wavelet. The equi-angular or HEALPix implementations of our algorithm are used independently on the two corresponding maps. For coherence with the studied scalar spherical harmonics transforms codes, the complete equi-angular implementation is coded in C, while the HEALPix implementation is coded in Fortran90.

For a given scale  $a \in \mathbb{R}_+^*$ , the angular size of our dilated wavelets  $\Psi_a$  on the sphere is defined as twice the dispersion of the corresponding Gaussian. Fifteen scales are selected corresponding to angular sizes of the second Gaussian derivative lying between 20 arcminutes and 60 degrees:  $a_1 \rightarrow 20'$ ,  $a_2 \rightarrow 40'$ ,  $a_3 \rightarrow 1^\circ$ ,  $a_4 \rightarrow 5^\circ$ ,  $a_5 \rightarrow 10^\circ$ ,  $a_6 \rightarrow 15^\circ$ ,  $a_7 \rightarrow 20^\circ$ ,  $a_8 \rightarrow 25^\circ$ ,  $a_9 \rightarrow 30^\circ$ ,  $a_{10} \rightarrow 35^\circ$ ,  $a_{11} \rightarrow 40^\circ$ ,  $a_{12} \rightarrow 45^\circ$ ,  $a_{13} \rightarrow 50^\circ$ ,  $a_{14} \rightarrow 55^\circ$ ,  $a_{15} \rightarrow 60^\circ$ . The analytical expression of the second Gaussian derivative wavelet as a function of the scale  $a$  may be found in (Wiaux et al. 2005). From a practical point of view, the wavelet is first sampled on the sphere in each pixelization, and the corresponding spherical harmonics coefficients  $(\hat{\Psi}_a)_{lm}$  are calculated by direct spherical harmonics transform at each scale.

The wavelet coefficients resulting from the directional correlation of the signal with the second Gaussian derivative at each scale  $a$  read as  $W_{\Psi}^T(\chi, \omega_0, a) = \langle R(\rho) \Psi_a | T \rangle$ , for  $\rho = (\varphi_0, \theta_0, \chi)$ , and  $\omega_0 = (\varphi_0, \theta_0)$ . The coefficients resulting from the standard correlations with the corresponding basis filters defined in (20) read  $W_{\Psi_m}^T(\omega_0, a) = \langle R(\omega_0) \Psi_{ma} | T \rangle$ , for  $1 \leq m \leq 3$ , and with  $\Psi_{1a} = \Psi_a^{\partial_x^2(\text{gauss})}$ ,  $\Psi_{2a} = \Psi_a^{\partial_y^2(\text{gauss})}$ , and  $\Psi_{3a} = \Psi_a^{\partial_x \partial_y(\text{gauss})}$ . The steerability relation (21) therefore explicitly reads

$$W_{\Psi}^T(\chi, \omega_0, a) = \sum_{m=1}^3 k_m(\chi) W_{\Psi_m}^T(\omega_0, a), \quad (43)$$

with the weights  $k_1(\chi) = \cos^2 \chi$ ,  $k_2(\chi) = \sin^2 \chi$ , and  $k_3(\chi) = \sin 2\chi$  given in (19). At each of the fifteen scales considered, the coefficients  $W_{\Psi_m}^T(\omega_0, a)$  gather all the information necessary to compute the directional correlation of the signal with the second Gaussian derivative. These coefficients are computed as functions on the sphere, up to the band limit  $L = 1024$ .

On the one hand, the overall computation times at each scale for the coefficients  $W_{\Psi_m}^T(\omega_0, a)$  of the three basis filters ( $1 \leq m \leq 3$ ) are of the order of  $7.1 \times 10^2$  seconds in the equi-angular implementation on a 2.20 GHz Intel Pentium Xeon CPU with 2 Gb of RAM memory. The same calculation takes  $2.1 \times 10^2$  seconds in the HEALPix implementation with zero iteration ( $i = 0$ ) for the direct transforms. These values may directly be inferred from the computation times reported in

<sup>4</sup> See cmbfast.org for documentation (CMBFAST4.5.1 software).

Table 1 for the scalar spherical harmonics transforms. Indeed, the second Gaussian derivative contains the frequencies  $n = \{0, \pm 2\}$  and  $|n| + 1$  inverse scalar spherical harmonics are required for each spin-weighted transform in (29). Let us also recall that opposite spins are grouped by the algorithm before applying the scalar spherical harmonics transforms. For each of the three basis filters, four inverse scalar transforms (one at spin 0 and three at spin 2) therefore add up to the direct scalar transform of the filter. Also adding the direct scalar transform of the signal, a total of four direct scalar transforms and twelve inverse scalar transforms are required, which leads to a very good estimation of the overall computation times reported above.

On the other hand, the relative precision of the equi-angular and HEALPix implementations may be probed quantitatively through the calculation of the mean and variance of the wavelet coefficients at each scale  $a$  and each direction  $\chi$ , respectively

$$\begin{aligned} \mu_{\Psi}^T(\chi, a) &= \frac{1}{4\pi} \int_{S^2} d\Omega_0 W_{\Psi}^T(\chi, \omega_0, a) \\ [\sigma_{\Psi}^T]^2(\chi, a) &= \frac{1}{4\pi} \int_{S^2} d\Omega_0 |W_{\Psi}^T(\chi, \omega_0, a) - \mu_{\Psi}^T(\chi, a)|^2. \end{aligned} \quad (44)$$

From relation (43), those moments are explicitly given from the means and (co-)variances of the standard correlations at each scale  $a$ , respectively, as

$$\begin{aligned} \mu_{\Psi}^T(\chi, a) &= \sum_{m=1}^3 k_m(\chi) \mu_m^T(a) \\ [\sigma_{\Psi}^T]^2(\chi, a) &= \sum_{m, m'=1}^3 k_m^*(\chi) k_{m'}(\chi) \sigma_{mm'}^T(a), \end{aligned} \quad (45)$$

with

$$\begin{aligned} \mu_m^T(a) &= \frac{1}{4\pi} \int_{S^2} d\Omega_0 W_{\Psi_m}^T(\omega_0, a) \\ \sigma_{mm'}^T(a) &= \frac{1}{4\pi} \int_{S^2} d\Omega_0 (W_{\Psi_m}^T(\omega_0, a) - \mu_{\Psi_m}^T(a))^* \\ &\quad (W_{\Psi_{m'}}^T(\omega_0, a) - \mu_{\Psi_{m'}}^T(a)). \end{aligned} \quad (46)$$

All these quantities are defined from the directional correlation of a real signal with a real wavelet, and are therefore themselves real. Notice that quadrature rules need to be applied in order to compute the latter integrals on both pixelizations. On equi-angular grids, the sampling theorem discussed in §4 equivalently states that the integral of a scalar function on the sphere with a band limit  $2L$  may be computed exactly as a weighted sum of its sampled values on  $2L \times 2L$  equi-angular grids. The quadrature weights are the same as those applied for the computation of spherical harmonics coefficients (Driscoll & Healy 1994). On HEALPix grids, the integral of a function on the sphere is simply approximated by the sum of its sampled values, as all pixels have the same area. These rules are applied for the computation of the integrals  $\mu_m^T(a)$  and  $\sigma_{mm'}^T(a)$  on the sphere, at each of the fifteen scales considered.

Figure 1 represents the six spectra  $\sigma_{mm'}^T(a)$  computed in the equi-angular and HEALPix implementations, as functions of the scale. The top panel represents the three variances  $\sigma_{mm}^T(a)$ , with  $1 \leq m \leq 3$ . The bottom panel represents the three covariances  $\sigma_{mm'}^T(a)$  with  $1 \leq m \neq m' \leq 3$ . For any of

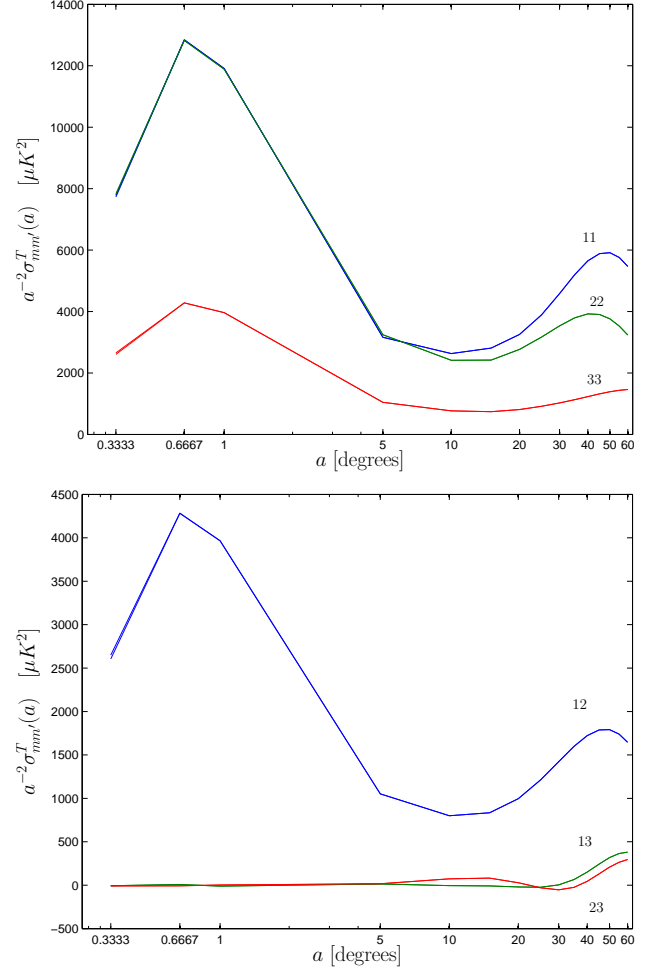


FIG. 1.— Comparison of the relative precision of the equi-angular and HEALPix implementations of the fast directional correlation algorithm. The six spectra associated with the wavelet coefficients from the directional correlation of a simulated CMB temperature map with the second Gaussian derivative wavelet are shown. The spectra, normalized as  $a^{-2} \sigma_{mm'}^T(a)$  with  $1 \leq m, m' \leq 3$ , are given in  $\mu K^2$  as functions of the wavelet scale  $a$ , converted in terms of angular size in degrees. The top panel represents the variances  $\sigma_{11}^T(a)$ ,  $\sigma_{22}^T(a)$ , and  $\sigma_{33}^T(a)$ . The bottom panel represents the covariances  $\sigma_{12}^T(a)$ ,  $\sigma_{13}^T(a)$ , and  $\sigma_{23}^T(a)$ . For all six spectra and at any of the fifteen scales considered, the maximum relative difference between the two implementations is bounded by 1.9%. The equi-angular and HEALPix curves are therefore indistinguishable.

those six spectra, at the first scale  $a_1 \rightarrow 20'$ , the maximum relative difference between the values arising from the equi-angular and HEALPix implementations is bounded by 1.9%. At that small scale, the assumption that the wavelet filter is band-limited at  $L$  is not perfect anymore. The wavelet is not perfectly well sampled on the grids considered. Consequently, aliasing errors can occur in both the equi-angular and HEALPix implementations, which explain the discrepancy between the spectra. For the remaining fourteen scales, the maximum relative difference between the spectra from the equi-angular and HEALPix implementations drops below 0.07%. This remaining difference may be attributed to the calculation of the scalar spherical harmonics transforms in the HEALPix implementation, which is approximate even for band-limited signals and filters. This discrepancy is indeed coherent with the relative root mean square error on the spherical harmonics transform, estimated at 0.24% in Table 2 for

HEALPix with zero iteration ( $i = 0$ ), and at  $L = 1024$ . We also know that this already very good precision of the HEALPix implementation can be enhanced using at least one iteration ( $i \geq 1$ ), at the price of an increased computation time. This would reduce the relative differences with the theoretically exact equi-angular implementation.

## 6. CONCLUSION

We introduced a fast algorithm for the directional correlation of band-limited signals with band-limited steerable filters on the sphere. The *a priori* asymptotic complexity associated with the directional correlation is  $\mathcal{O}(L^5)$ , where  $2L$  stands for the square-root of the number of sampling points on the sphere, also setting a band limit  $L$  for the signals and filters considered. The use of steerable filters allows to compute the directional correlation uniquely in terms of direct and inverse scalar spherical harmonics transforms. The overall asymptotic complexity is correspondingly reduced to the asymptotic complexity of scalar spherical harmonics transforms, that is  $\mathcal{O}(L^3)$ . We also emphasized that an  $\mathcal{O}(L^2 \log_2^2 L)$  asymptotic complexity may be achieved on equi-angular pixelizations if associated Legendre polynomials are pre-calculated. We thoroughly compared the implementations of the scalar spherical harmonics transforms on HEALPix and equi-angular grids, in terms of memory requirements, numerical stability, and computation times. First, the memory requirements are easily accessible. Second, the SpharmonicKit implementation on equi-angular grids based on an exact algorithm proposed by Driscoll and Healy reaches the computer's numerical precision. The exactness of the calculation relies on a sampling theorem for scalar functions on equi-angular grids on the sphere. The already good precision of the HEALPix implementation of the scalar spherical harmonics transform may be enhanced through an iterative process, but never reaches the level achieved on equi-angular grids. Third, the computation times for the  $\mathcal{O}(L^3)$  scalar transform of maps of several megapixels on the sphere ( $L \simeq 10^3$ ) are reduced from years to tens of seconds on a single standard computer in

both the equi-angular and HEALPix implementations. The equi-angular implementation is slightly less rapid than the HEALPix implementation with zero iteration ( $i = 0$ ), but becomes more rapid as soon as at least one iteration ( $i \geq 1$ ) is considered in the HEALPix scheme. The computation of the directional correlation of multiple signals or simulations with steerable filters is thereby rendered easily affordable at high resolutions.

In the perspective of the scale-space analysis of the CMB temperature ( $T$ ) and polarization ( $E$  and  $B$ ) anisotropies, the wavelet processing of the CMB data is therefore easily affordable at the high resolutions of the WMAP and Planck experiments. The identification of possible local non-Gaussianity or statistical anisotropy signatures, or foreground emissions, is accessible with the same high precision in both position and local direction on the sphere. The low computation times and very good precision of the equi-angular and HEALPix implementations of our algorithm was clearly illustrated in that context through a wavelet decomposition of a simulated three-year WMAP temperature map of several megapixels.

The generic algorithm developed for the fast directional correlation on the sphere may also find other applications, notably in the analysis of asymmetric beam effects on the CMB temperature and polarization data, or well beyond cosmology.

The authors acknowledge the use of the LAMBDA archive, and of the HEALPix and CMBFAST softwares. They wish wish to thank J.-P. Antoine, B. Barreiro, and E. Martínez-González for valuable comments and discussions. They acknowledge support of the HASSIP (Harmonic Analysis and Statistics for Signal and Image Processing) European research network (HPRN-CT-2002-00285). Y. W. acknowledges support of the Swiss National Science Foundation (SNF) under contract No. 200021-107478/1. He is also postdoctoral researcher of the Belgian National Science Foundation (FNRS). P. V. was supported by the Spanish MEC project ESP2004-07067-C03-01.

## REFERENCES

- Abramowitz, M., & Stegun, I. 1965, Handbook of mathematical functions (New York: Dover Publications Inc.)
- Brink, D. M., & Satchler, G. R. 1993, Angular Momentum (Third Edition; Oxford: Clarendon Press)
- Bülöw, T., & Daniilidis, K. 2001, technical report (MS-CIS-01-37)
- Bülöw, T. 2002, in Proc. 24th DAGM Symposium for Pattern Recognition 2449, ed. L. Van Gool, (Heidelberg: Springer-Verlag), 609
- Carmeli, M. 1969, J. Math. Phys., 10, 569
- Challinor, A., Fosalba, P., Mortlock, D., Ashdown, M., Wandelt, B., & Górski, K. 2000, Phys. Rev. D, 62, 123002
- Cruz, M., Martínez-González, E., Vielva, P., & Cayón, L. 2005, MNRAS, 356, 29
- Doroshkevich, A. G., Naselsky, P. D., Verkhodanov, O. V., Novikov, D. I., Turchaninov, V. I., Novikov, I. D., Christensen, P. R., & Chiang, L.-Y. 2005a, Int. J. Mod. Phys. D, 14, 275
- Doroshkevich, A. G., Naselsky, P. D., Verkhodanov, O. V., Novikov, D. I., Turchaninov, V. I., Novikov, I. D., Christensen, P. R., & Chiang, L.-Y. 2005b, preprint (astro-ph/0501494)
- Driscoll, J. R., & Healy, D. M., Jr. 1994, Adv. in Appl. Math., 15, 202
- Freeman, W. T., & Adelson, E. H. 1991, IEEE Trans. Pattern Anal. Machine Intell., 13, 891
- Goldberg, J. N., Macfarlane, A. J., Newman, E. T., Rohrlach, F., & Sudarshan, E. C. G. 1967, J. Math. Phys., 8, 2155
- Górski, K. M., Hivon, E., Banday, A. J., Wandelt, B. D., Hansen, F. K., Reinecke, M., & Bartelman, M. 2005, ApJ, 622, 759
- Healy, D. M., Jr., Rockmore, D. N., Kostelec, P. J., & Moore, S. 2003, J. Fourier Anal. and Applic., 9, 341
- Healy, D. M., Jr., Kostelec, P. J., & Rockmore, D. N. 2004, Adv. in Comput. Math., 21, 59
- Hu, W., & White, M. 1997, Phys. Rev. D, 56, 596
- Kamionkowski, M., Kosowsky, A., & Stebbins, A. 1997a, Phys. Rev. Lett., 78, 2058
- Kamionkowski, M., Kosowsky, A., & Stebbins, A. 1997b, Phys. Rev. D, 55, 7368
- Kosowsky, A. 1996, Ann. Phys., 246, 49
- Kostelec, P. J., Maslen, D. K., Rockmore, D. N., & Healy, D. M., Jr. 2000, J. Comput. Phys., 162, 514
- Kostelec, P. J., & Rockmore, D. N. 2003, technical report (SFI-03-11-060)
- Maslen, D. K., & Rockmore, D. N. 1997a, J. American Math. Soc., 10, 169
- Maslen, D. K., & Rockmore, D. N., 1997b, in Proc. DIMACS Workshop on Groups and Computation 28, ed. L. Finkelstein, & W. Kantor, (Providence: American Math. Soc.), 183
- McEwen, J. D., Hobson, M. P., Lasenby, A. N., & Mortlock, D. J. 2005a, MNRAS, 359, 1583
- McEwen, J. D., Hobson, M. P., Lasenby, A. N., & Mortlock, D. J. 2005b, preprint (astro-ph/0506308)
- Mukherjee, P., & Wang, Y. 2004, ApJ, 613, 51
- Newman, E. T., & Penrose, R. 1966, J. Math. Phys., 7, 863
- Ng, K.-W. 2005, Phys. Rev. D, 71, 083009
- Page, L., et al. 2003, ApJS, 148, 233
- Risbo, T. 1996, J. Geodesy, 70, 383
- Roukema, B. F., & Lew, B. 2004, preprint (astro-ph/0409533)
- Seljak, U., & Zaldarriaga, M. 1997, Phys. Rev. Lett., 78, 2054
- Simoncelli, E. P., Freeman, W. T., Adelson, E. H., & Heeger, D. J. 1992, IEEE Trans. Information Theory, 38, 587

- Spergel, D. N., et al. 2003, *ApJS*, 148, 175
- Spergel, D. N., et al. 2006, preprint ([lambda.gsfc.nasa.gov](http://lambda.gsfc.nasa.gov))
- Varshalovich, D. A., Moskalev, A. N., & Khersonskii, V. K. 1989, *Quantum Theory of Angular Momentum* (First Edition Reprint; Singapore: World Scientific)
- Vielva, P., Martínez-González, E., Barreiro, R. B., Sanz, J. L., & Cayón, L. 2004, *ApJ*, 609, 22
- Wandelt, B. D., & K. M. Górski 2001, *Phys. Rev. D*, 63, 123002
- Wiaux, Y., Jacques, L., & Vandergheynst, P. 2005, *ApJ*, 632, 15
- Zaldarriaga, M., & Seljak, U. 1997, *Phys. Rev. D*, 55, 1830